

Real-time 10,000 km Straight-line Transmission using a Software-defined GPU-Based Receiver

Sjoerd van der Heide, *Student Member, IEEE*, Ruben S. Luis, *Senior Member, IEEE*, Benjamin J. Puttnam, *Member, IEEE*, Georg Rademacher, *Senior Member, IEEE*, Ton Koonen, *Fellow, IEEE*, Satoshi Shinada, *Member, IEEE*, Yohinari Awaji, *Member, IEEE*, Hideaki Furukawa, *Member, IEEE*, Chigo Okonkwo, *Senior Member, IEEE*

Abstract—Real-time 10,000 km transmission over a straight-line link is achieved using a software-defined multi-modulation format receiver implemented on a commercial off-the-shelf general-purpose graphics processing unit (GPU). Minimum phase 1 GBaud 4-ary quadrature amplitude modulation (QAM) signals are transmitted over 10,000 km and successfully received after detection with a Kramers-Kronig (KK) coherent receiver. 8-, 16-, 32-, and 64-QAM are successfully transmitted over 7600, 5600, 3600, and 1600 km, respectively.

Index Terms—Real-time, Kramers-Kronig, long-haul, GPU.

I. INTRODUCTION

Real-time digital signal processing (DSP) for optical communications has traditionally taken form of application-specific integrated circuits (ASICs) and field-programmable gate arrays (FPGAs) [1]–[3]. Graphics processing units (GPUs) have experienced more than a decade of steady exponential growth in terms of computing capability (45% year-on-year [4]) and energy efficiency (25% year-on-year [5]), making them a potential alternative to ASICs and FPGAs. These improvements combined with low development effort and rapid turnaround have enabled recent demonstrations of real-time DSP for optical communications [6]–[14]. These demonstrations include real-time forward error correction (FEC) decoding [6], [7], physical-layer functionality [8]–[10], and differential quaternary phase-shift-keying (DQPSK) detection [11]. We introduced a real-time flexible multi-modulation format receiver for directly detected pulse-amplitude modulated signals and Kramers-Kronig (KK) [15] coherently detected minimum phase (MP) [15] QAM signals and verified its operation over a field-deployed link in [12], [13]. The potential to support long distance links with digital compensation of linear transmission impairments, such as chromatic dispersion,

was further demonstrated in [14], where this system was shown to support transmission up to 10,000 km.

This letter revisits and extends the results presented in [14]. A real-time flexible multi-modulation format receiver is experimentally evaluated for long-haul optical communications using a 10,000 km straight-line link consisting of 100 spans with an average length of 100 km. The real-time DSP is implemented on a commercial off-the-shelf GPU and is able to receive MP N-QAM signals detected with a KK coherent receiver. The signal processing chain includes the KK algorithm as well as equalization, compensating for chromatic dispersion in frequency domain. Successful transmission of 1 GBaud 4-, 8-, 16-, 32-, 64-QAM is shown up to 10,000 km, 7600 km, 5600 km, 3600 km and 1600 km, respectively. In addition to the outcomes presented in [14], we address achievable throughput as the critical parameter of optimization for software-defined multi-modulation format systems. Furthermore, to the authors' knowledge, the use of MP signals for transmission over such long distances has never been performed, we address the impact of carrier-to-signal power ratio (CSPR) for this transmission scenario. The results demonstrate the potential for GPUs in long-haul optical communication systems, in particular for datacenter-to-datacenter applications without the use of third-party hardware.

II. EXPERIMENTAL SETUP

Fig. 1 shows the experimental setup, including the real-time DSP chain. The MP N-QAM test signals are modulated onto the lightwave originating from a 100 kHz external cavity laser (ECL) by an in-phase and quadrature modulator (IQM) driven by a 2-channel 12 GS/s arbitrary-waveform generator (AWG), equipped with RF drivers. The modulator arms are kept at the minimum optical output bias point using bias tees and voltage sources. To ensure that the signal is MP, a carrier tone is inserted digitally with CSPR controlled by modifying the power of the carrier tone with respect to the N-QAM signal. Note that at low CSPR, the minimum-phase condition is occasionally violated, leading to reconstruction errors [15]. Between the 1 GBaud 1% roll-off root-raised-cosine (RRC) N-QAM signal with frequency components up to 0.505 GHz and the digitally-inserted carrier tone at 0.516 GHz, a small gap of only 11 MHz is left. An investigation revealed this relatively small gap to balance the trade-off between increased KK reconstruction

Sjoerd van der Heide, Ton Koonen, and Chigo Okonkwo are with the High-Capacity Optical Transmission Laboratory, Electro-Optical Communications Group, Eindhoven University of Technology, PO Box 513, 5600 MB, Eindhoven, the Netherlands. (e-mail: s.p.v.d.heide@tue.nl, c.m.okonkwo@tue.nl, a.m.j.koonen@tue.nl). Ruben S. Luis, Benjamin J. Puttnam, Georg Rademacher, Satoshi Shinada, Yohinari Awaji, and Hideaki Furukawa are with the National Institute of Information and Communications Technology, Photonic Network System Laboratory, 4-2-1, Nukui-Kitamachi, Koganei, Tokyo, 184-8795, Japan (e-mail: rluis@nict.go.jp).

Manuscript received xxxx; revised xxxx; accepted xxxx. Date of publication xxxx. This work was partly supported by the Dutch NWO Gravitation Program on Research Center for Integrated Nanophotonics under Grant GA 024.002.033.

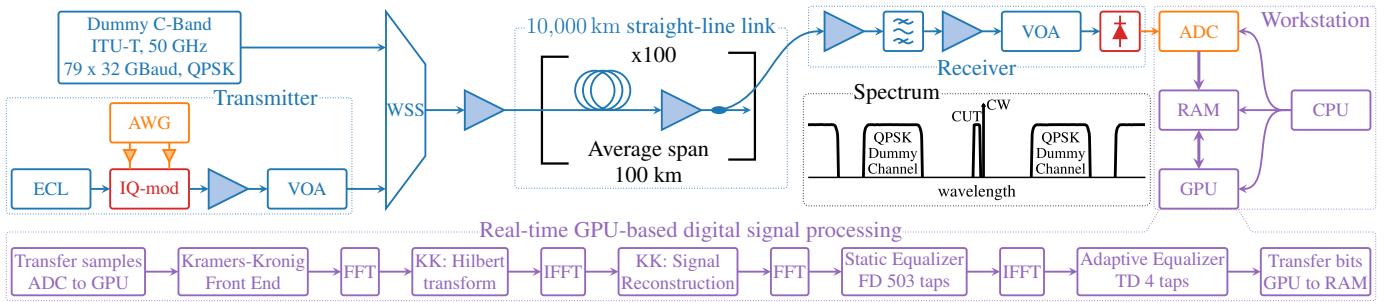


Fig. 1: Experimental setup including the 10,000 km straight-line link and a schematic of the main DSP blocks.

errors due to increased signal-signal beat interference (SSBI) at smaller gaps versus increased KK reconstruction errors due to bandwidth limitations of the employed receiver at larger gaps. With other equipment, the optimum may differ.

The MP N-QAM test signal is amplified and combined by a wavelength selective switch (WSS) with a dummy band of 79 32 GBaud quaternary phase-shift-keying (QPSK) signals, spaced according to the 50 GHz ITU-T grid with a gap at 1550.116 nm for the test signal to emulate full C-band transmission, see the schematic *Spectrum* inset in Fig. 1. The wavelength-division multiplexing (WDM) signal is amplified and transmitted over the 100-span straight-line link. The average span length is 100 km with WSSs placed every 20 spans to flatten the transmission spectrum. Note that this is not a recirculating loop experiment, therefore, the link physically contained 10,000 km of fiber. The transmission fiber was designed for submarine transmission and has a loss of 0.154 dB/km and an effective mode-area of $112 \mu\text{m}^2$. The total launch power at the input of each span is 20 dBm and cannot be varied due to setup constraints. To investigate the influence of launch power on nonlinearities and noise, the launch power of the test signal relative to the dummy channels is varied using a variable optical attenuator (VOA). Monitoring taps at various points along the link allowed for evaluation at distances up to 10,000 km. At the receiver, the tapped WDM signal is amplified and the test signal is filtered using a 5 GHz optical bandpass filter. Another erbium-doped fiber amplifier (EDFA) amplifies the test signal with a VOA controlling the power into a 6.5 GHz photodiode. The electrical signal is sent to the workstation and digitized by a 12-bit 4 GS/s 1 GHz analog-to-digital converter (ADC) and processed in real-time on the GPU, which has a maximum rated power of 250 W.

The real-time DSP is schematically shown in Fig. 1 and its GPU-based implementation is described in detail in [13]. The ADC transfers buffers of samples to the GPU using direct memory access (DMA) over an 8-lane PCIe Gen3 interface. Each buffer contains 2^{22} samples and is subdivided into 8192 blocks for 100% overlap-save frequency domain (FD) processing. Separate GPU processing streams are used for each buffer to facilitate greater parallelization. The signal processing starts with a GPU kernel handling the overlap with the last block of the previous buffer to make a contiguous stream of samples available for signal processing. This kernel also converts the samples from 12-bit fixed point to 32-bit floating point representation and handles the KK front-

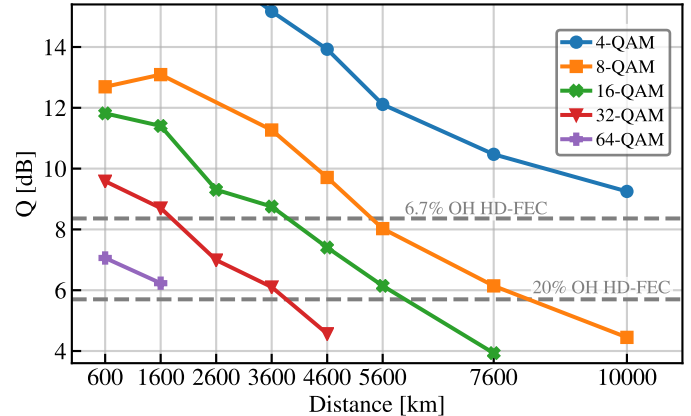


Fig. 2: Q-factor versus distance for various N-QAM formats.

end operations consisting of the square root and logarithm operations. Then, a 1024-point 100% overlap-save fast Fourier transform (FFT) pair enables a FD Hilbert transformation to retrieve the phase of the optical signal. Note that these operations, through the utilization of millions of threads, leverage the massive parallelization offered by GPUs, next to the parallelization offered by parallel processing streams. The retrieved phase is combined with the amplitude to reconstruct the optical field [15], which is subsequently downshifted to DC for further processing. Another pair of FFTs enables FD static equalization and resampling from 4 to 2 samples-per-symbol. The static equalizer is optimized off-line using 203 taps at 2 samples per symbol. Finally, the signal is filtered by 4-tap adaptive decision-directed least mean square (DD-LMS) widely-linear [16] time domain (TD) equalizer capable of correcting for modulator IQ-imbances. The decisions of the adaptive equalizer are demapped and transferred to random-access memory (RAM). Since the GPU is able to process incoming digitized buffers at a rate faster than they are produced by the ADC, this receiver is considered operating in real time. Note that overlap between buffers is carefully handled as explained here and in [13], enabling a fully contiguous data stream to be processed and transferred to RAM, differentiating this receiver from a very fast block-wise off-line DSP. Large buffers allow for many threads to process data in parallel and reduce overhead penalties, leading to lower development effort but increased latency. Future implementations can lower latency through careful optimization of buffer size and efforts to reduce overhead. Although GPU-based FEC decoding is

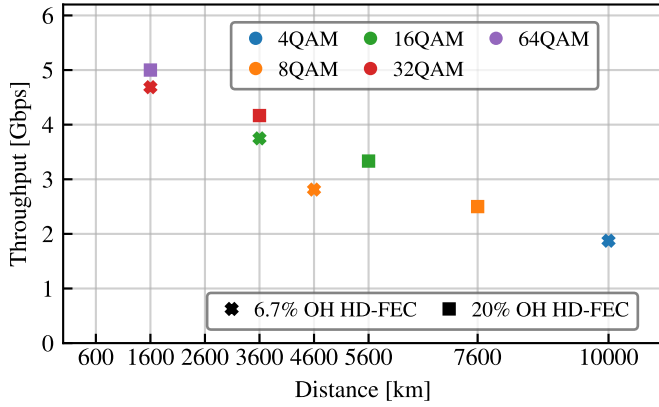


Fig. 3: Net throughput versus distance.

possible [6], [7], it is considered beyond the scope of this work. However, to limit FEC complexity, we only assume hard decision FECs. Since the storage media in our workstation computer are not fast enough to save the data stream in real time, results were saved to RAM. The size of our RAM limited the real time trace lengths reported in this paper to about 21 seconds.

III. RESULTS AND DISCUSSION

Fig. 2 shows the Q-factor as a function of distance for all considered N-QAM formats. CSRR and relative launch power were optimized for each data point. 4-QAM reaches the 6.7% overhead (OH) hard decision forward error correction (HD-FEC) [17] threshold at 10,000 km and since the physical link was not longer, we could not measure farther. If a 20% OH HD-FEC [17] is employed, 8-QAM can be successfully transmitted over up to 7600 km. Using this same threshold, 16-, 32-, 64-QAM can reach 5600 km, 3600 km and 1600 km, respectively. The net throughput for all formats and both HD-FEC thresholds is plotted against distance in Fig. 3. Note that this is not interpolated, the farthest data point above the HD-FEC threshold is plotted for each format. Using the software-defined flexible multi-modulation format receiver, a suitable format can be chosen for each distance, maximizing the net throughput.

Fig. 4 shows the Q-factor versus relative launch power for all considered modulation formats. It shows that the power of the test channels needs to be well below that of the dummy channels for maximum performance. This suggests a dominant impact of self-phase modulation (SPM), perhaps on the MP carrier tone. The optimum shifts with format and distance. Therefore, this effect is investigated for 4-QAM at 5600 km and 10,000 km in Fig. 5 for various CSRRs. At 10,000 km, the optimal relative launch power for 4-QAM is about 2 dB lower than at 5600 km. This confirms the optimal launch power is dependent on distance.

Fig. 5 also shows the CSRR trade-off between nonlinearities and noise. Since a higher CSRR has more power in the carrier tone and less power in the N-QAM signal, the influence of noise is increased. Therefore, the optimal launch power is higher for higher CSRRs as shown in the figure. At high launch

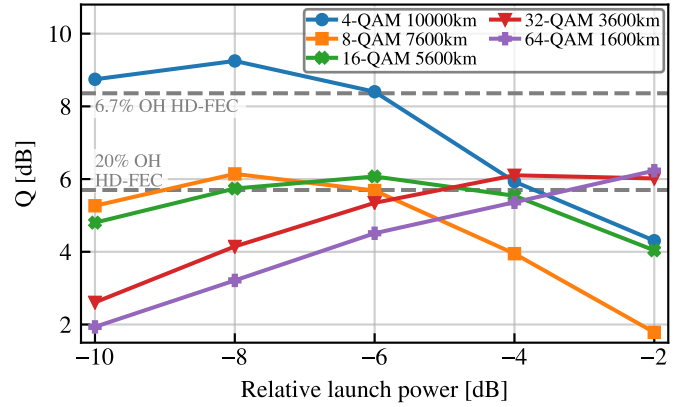


Fig. 4: Q-factor versus relative launch power for various formats at their FEC-limit distance.

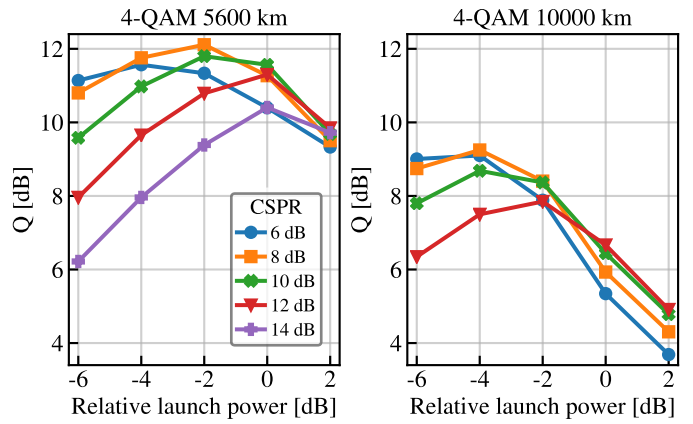


Fig. 5: Q-factor versus relative launch power for 4-QAM.

powers, nonlinear interactions degrade the signal leading to a drop in performance.

The optimum launch power dependence on transmission distance is further investigated in Fig. 6, where the relative launch power with optimized CSRR leading to the highest Q-factor is plotted as a function of distance for both 4-, and 32-QAM. For both formats, the optimal launch power decreases substantially with transmission distance. This is a surprising outcome since in conventional coherent transmission systems, optimal launch power tends to remain independent of transmission distance because signal degradation due to fiber nonlinearities and noise scale at a similar rate for a fully populated C-band [18]. However, in the case of an MP N-QAM signal detected using a KK coherent receiver, the nonlinear interactions between signal and carrier tone seem to scale at a higher rate than noise with distance, leading to a lower optimal launch power with greater transmission distance. Further investigation into MP signal degradation due to nonlinear fiber interactions is required to fully describe this behavior.

Finally, Fig. 7 shows continuous real-time traces for 4-, 8-, and 16-QAM at 7600 km transmission distance. The Q-factor is estimated from bit error rate (BER) and is averaged over intervals of 21 ms. The 21 second traces show stable short-term averaged Q-factors, even for 16-QAM which operates in a very low Q-factor regime, demonstrating the robustness of

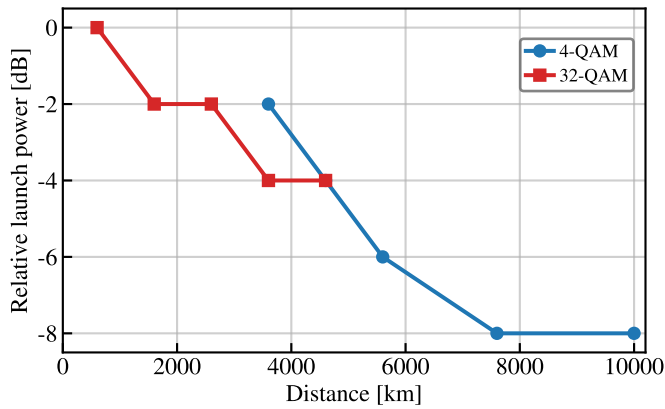


Fig. 6: Optimal relative launch power versus distance.

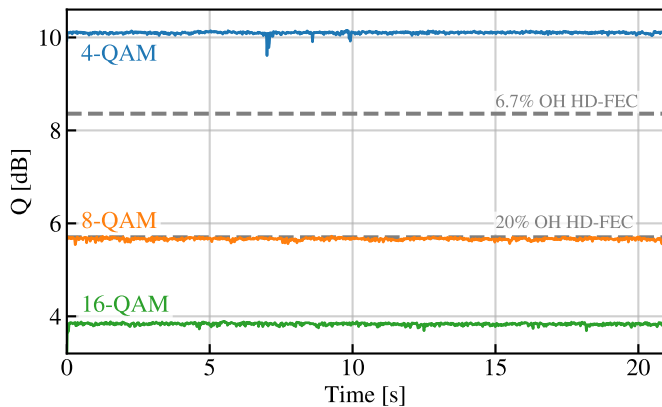


Fig. 7: Continuous real-time traces at 7600 km.

the signal processing. This shows the receiver is capable of sustained operation with the main limitation imposed by the RAM capacity of the workstation used for the experimental validation. Power consumption of the receiver concept is expected to decrease as energy efficiency of GPUs continues to improve.

IV. CONCLUSIONS

A flexible real-time multi-modulation format receiver using a commercial off-the-shelf GPU is experimentally evaluated for long-haul optical communication. 1 GBaud minimum phase (MP) N-QAM signals are successfully transmitted over an experimental 10,000 km straight-line link and detected using a KK coherent receiver. The real time signal processing includes the KK algorithm as well as digital chromatic dispersion compensation, enabling successful transmission of 4-QAM up to 10,000 km. 8-, 16-, 32-, 64-QAM reach 7600 km, 5600 km, 3600 km and 1600 km of transmission, respectively. CSRR and launch power are optimized for each format and transmission distance. The result of this optimization is analyzed and we show that the nonlinear behavior of MP signals is substantially different from conventional coherent systems. Furthermore, we show that our system is capable of sustained operation in 21 second long continuous real-time traces, showing stable performance of 4-, 8-, and 16-QAM

over 7600 km. These results demonstrate the potential for employing GPUs in long-haul optical transmission systems.

REFERENCES

- [1] S. Randel, S. Corteselli, D. Badini, *et al.*, "First real-time coherent MIMO-DSP for six coupled mode transmission," in *2015 IEEE Photonics Conference (IPC)*, 2015. DOI: 10.1109/IPC.2015.7323761.
- [2] S. Beppu, K. Igarashi, H. Mukai, *et al.*, "Real-time strongly-coupled 4-core fiber transmission," in *Optical Fiber Communication Conference (OFC) 2020*, Optical Society of America, 2020, Th3H.2. DOI: 10.1364/OFC.2020.Th3H.2.
- [3] S. Beppu, K. Igarashi, M. Kikuta, *et al.*, "Weakly coupled 10-mode-division multiplexed transmission over 48-km few-mode fibers with real-time coherent MIMO receivers," *Opt. Express*, vol. 28, no. 13, pp. 19 655–19 668, Jun. 2020. DOI: 10.1364/OE.395415.
- [4] P. J. Winzer and D. T. Neilson, "From Scaling Disparities to Integrated Parallelism: A Decathlon for a Decade," *J. of Lightw. Technol.*, vol. 35, no. 5, pp. 1099–1115, Mar. 2017.
- [5] Y. Sun *et al.*, "Summarizing CPU and GPU Design Trends with Product Data," en, *arXiv:1911.11313 [cs]*, Nov. 2019, arXiv: 1911.11313.
- [6] R. Li, J. Zhou, Y. Dou, *et al.*, "A multi-standard efficient column-layered LDPC decoder for Software Defined Radio on GPUs," in *2013 IEEE 14th Workshop on Signal Processing Advances in Wireless Communications (SPAWC)*, 2013, pp. 724–728. DOI: 10.1109/SPAWC.2013.6612145.
- [7] T. Suzuki, S. Kim, J. Kani, *et al.*, "Demonstration of 10-Gbps Real-Time Reed–Solomon Decoding Using GPU Direct Transfer and Kernel Scheduling for Flexible Access Systems," *Journal of Lightwave Technology*, vol. 36, no. 10, pp. 1875–1881, 2018. DOI: 10.1109/JLT.2018.2793938.
- [8] T. Suzuki, S. Kim, J. Kani, *et al.*, "10-Gb/s Software Implementation of Burst-Frame Synchronization Using Array-Access Bitshift and Dual-Stage Detection for Flexible Access Systems," *Journal of Lightwave Technology*, vol. 36, no. 23, pp. 5656–5662, 2018. DOI: 10.1109/JLT.2018.2870912.
- [9] T. Suzuki *et al.*, "Software Implementation of 10G-EPON Upstream Physical-Layer Processing for Flexible Access Systems," *J. of Lightw. Technol.*, vol. 37, no. 6, pp. 1631–1637, Mar. 2019.
- [10] T. Suzuki, S. Kim, J. Kani, *et al.*, "Demonstration of Fully Softwarized 10G-EPON PHY Processing on a General-Purpose Server for Flexible Access Systems," *Journal of Lightwave Technology*, vol. 38, no. 4, pp. 777–783, 2020. DOI: 10.1109/JLT.2019.2948333.
- [11] T. Suzuki *et al.*, "Real-Time Implementation of Coherent Receiver DSP Adopting Stream Split Assignment on GPU for Flexible Optical Access Systems," *J. of Lightw. Technol.*, vol. 38, no. 3, pp. 668–675, Feb. 2020.
- [12] S. P. van der Heide, R. S. Luis, B. J. Puttnam, *et al.*, "Real-time, Software-Defined, GPU-Based Receiver Field Trial," *ECOC We1E5*, 2020.
- [13] S. P. van der Heide, R. S. Luis, B. J. Puttnam, *et al.*, "Field Trial of a Flexible Real-Time Software-Defined GPU-Based Optical Receiver," *J. Lightwave Technol.*, vol. 39, no. 8, pp. 2358–2367, Apr. 2021.
- [14] S. P. van der Heide, R. S. Luis, B. J. Puttnam, *et al.*, "10,000 km Straight-line Transmission using a Real-time Software-defined GPU-Based Receiver," in *2021 Optical Fiber Communications Conference and Exhibition (OFC)*, 2021, pp. 1–3.
- [15] A. Mecozzi, C. Antonelli, and M. Shtaif, "Kramers Kronig coherent receiver," en, *Optica*, vol. 3, no. 11, p. 1220, Nov. 2016. DOI: 10.1364/OPTICA.3.001220.
- [16] E. P. da Silva and D. Zibar, "Widely Linear Equalization for IQ Imbalance and Skew Compensation in Optical Coherent Receivers," *Journal of Lightwave Technology*, vol. 34, no. 15, pp. 3577–3586, 2016.
- [17] E. Agrell and M. Secondini, "Information-Theoretic Tools for Optical Communications Engineers," in *2018 IEEE Photonics Conference (IPC)*, IEEE, Sep. 2018, pp. 1–5. DOI: 10.1109/IPC.2018.8527126.
- [18] P. Poggiolini, G. Bosco, A. Carena, *et al.*, "The gn-model of fiber non-linear propagation and its applications," *Journal of Lightwave Technology*, vol. 32, no. 4, pp. 694–721, 2014. DOI: 10.1109/JLT.2013.2295208.